Synthesis of Nano Thermal Barrier Coating For Turbines In Aircraft Engines

Indhumathi E.
Department of Aeronautical Engineering, RVS educational Trust's Group of Instituions, Dindigul, Tamilnadu

Abstract - Lanthanum zirconate (La2Zr2O7), ceramic was synthesized by the co precipitation method. The phase compositions, thermo physical properties and surface morphologies of these materials were investigated. The X-Ray Difractometer (XRD) results revealed that the compositions of all prepared ceramic materials were in the range of the synthesis of single La2Zr2O7 with pyrochlore structure. After the prepared ceramic powders were mechanically dry-milled, vacuum dried, at 1000 0C for 10 hours, the bulk density of the sample was measured by the Archimedes method with an immersion medium of deionized water. A high-temperature dilatometer, Differential Scanning Calorimeter (DSC) and laser thermal diffusivity method were used to analyze its thermal expansion coefficient, specific heat and thermal diffusivity. The results showed that, with the temperature increasing, the thermal expansion coefficient (TEC) of these ceramics increased, while the thermal conductivity decreased. These results imply that Lanthanum Zirconate (LZ) can be explored as the candidate material for the ceramic layer in TBCs system.

I. INTRODUCTION

Thermal barrier coatings (TBCs) are used to protect and insulate primarily metallic components when they are exposed to high temperatures. TBCs are used in a large extent to protect components from hot gas streams in e.g. gas turbine engines.

In industrial applications, where space is at a premium, thermal barrier coatings are commonly used to protect from heat loss (or gain). Especially in gas turbines and jet engines the turbine blades are covered with TBCs. Such turbine blades are made of super alloys and the TBC avoids melting, which allows to reach high gas inlet temperatures and enables a high energy conversion efficiency.

A TBC normally consists of a base material called the substrate, two layers over the substrate: 1) a ceramic top coat to provide thermal protection, and 2) a metal alloy bond coat to provide a thermal expansion gradation layer between the ceramic and metal alloy substrate, improve adhesion of the top coat, and protect the substrate from oxidation. To date, materials and engineering technology has struggled to find solutions to prevent the failure of thermal barrier coatings, in the form of chipping off the alloy substrate, which occurs after repeated thermal cycling. This failure is aggravated by the growth of an oxide layer between the thermal barrier top coat and the metal alloy bond coat[a]. The top coat is the insulation layer and should have a high wear resistance, good chemical and thermal stability and good heat insulating properties. During operation, a thermally grown oxide layer forms at the interface between the bond coat and the top coat.[1-3]

There are several basic requirements for a material to be used as a TBC: low thermal conductivity, high melting point, high thermal expansion coefficient, no phase transformation between room temperature and the operating temperature, low sintering rate, chemical inertness, high hardness and good adhesion to the substrate. With a high thermal expansion coefficient, low thermal conductivity, chemical- and thermal stability, yttria stabilized Zirconia (YSZ) is the most widely used material for TBCs today. However, this material has a limiting operation temperature due to sintering and phase transitions at elevated temperatures. Next generation TBCs will result in increased temperature exposures of the top coat and new materials may therefore be required. Lanthanum Zirconate (LZ) was recently proposed as a TBC candidate due to its promising properties: low sintering at high temperatures, no phase transitions, thermal and chemical stability, low thermal conductivity and no oxygen transparency. The drawback with LZ is the thermal expansion mismatch with the bond coat leading to spallation during temperature cycling. [4]

II. EXPERIMENTAL WORK

2.1 Substrate Preparation

The precursor solution was used to coat stainless steel substrates by use of spray pyrolysis. AISI 310 S was chosen as the substrate material in this work. AISI 310 S is an austenitic nickel-chromium based alloy 19-22% Ni, 24-26%Cr,0.08% max of C, balance Fe, 2% max Mn, 1.50% max Si, 0.03% S, 0.045% P [5]. The stainless steel substrates with a thickness of 2.5 mm were cut into geometries, quadratic (2.0 cm * 2.0cm) and then cleaned with ethanol.

2.2 Bond coating

Bond coating for the substrate is done by air plasma spraying.

2.2.1. Spray parameters – air plasma spraying

a) Plasma gases: These are used to generate the plasma jet. Their flow rates are needed.

Primary gas: Typically, argon or nitrogen

Secondary gases: Typically, helium and/or hydrogen. (Note: Use of hydrogen, in addition to helium will increase the heat transfer to the powder particles)

b) Plasma torch power

For most plasma spray systems (e.g. 9MC plasma spray controller system), the voltage or the current must be modulated to achieve the appropriate power. In addition to modulating the voltage or the current, the flow rate of the plasma gases must also be modulated.

For example, the operator may set the plasma gas flow rates constant and modulate the voltage input to the torch. The controller, in turn, will report the input current and power.

c) Torch velocity

Velocity of the torch may be programmed through the controller. It is usually reported in inches per second (IPS) or inches per minute (IPM). Slower velocities will produce thicker coatings per pass. Typically, the torch velocity is approximately 800 to 1200 IPM (340 mm/s to 510 mm/s).

d) Stand-off distance

Stand-off distance is the distance between the torch and the substrate. An appropriate stand-off distance will ensure that the powder particles are fully molten before deposition, and that the substrate does not overheat during spraying.

2.2.2. The technical specifications of air plasma spray

Gun	Nozzle	Argon [lit/min]		Hydrogen [lit/min]		Current [amp]	Voltage [volts]	Powder feed [gm/min]	Spray distance [inches]
		Pressure	Flow rate	Pressure	Flow rate				
3 MB	GH nozzle	75 - 100	80 - 90	50	15 - 18	500	60-70	30-45	2-3

Table 2.1: The technical specifications of air plasma spray

2.2.3. Spraying procedures

a) Start the dust collector system.

b) Initiate the robot. This step assumes that the robot has been programmed and verified.

c) Start the torch system. Enter the selected flow rates of the plasma gases and

voltage/current. Select the appropriate stand-off distance. Do this step with the torch away from the substrate (to the side).

d) If required, start the turntable system.

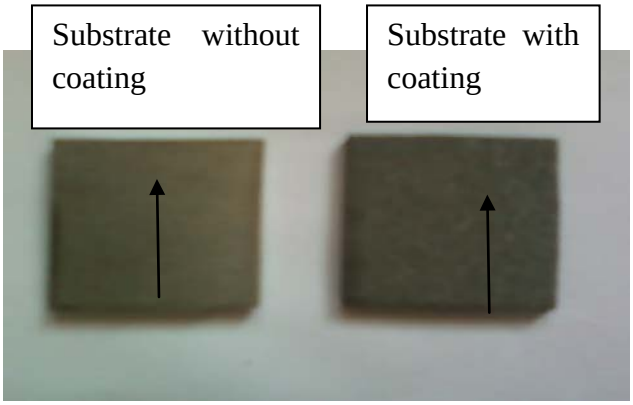

Fig 2.1.AISI 310S steel with and without bond coating

e) Pass the torch, without powder, over the substrate. The high speed of the high temperature jet will remove residual grit from the substrate surface.

f) Move the torch away from the substrate (e.g. to the side). Open the powder feed system. Do a visual verification of the presence of powder particles within the plasma jet.

g) Start the torch passes. The robot may be programmed to complete all the required passes. The passes may also be controlled by the operator at the controller.

h) Typically, 0.5 to 2 mils (0.0005 to 0.002 inches) thick layers are deposited per pass.

i) A pyrometer can be used to monitor the coating temperature during spraying. Coating temperatures should be maintained on the order of 140 to 160^{o}C. For metals, in particular, this will ensure that oxidation is kept at a minimum.

Oxidation reduces the overall quality of the coatings. It is suggested to adhere to these temperature limits for

ceramics. If needed, the surface temperature of ceramic coatings may be increased.

2.3 Synthesis of $La_2Zr_2O_7$

Chemicals	Formula	Purity	Suppliers
Lanthanum (III)nitrate hexa hydrate	$La(NO_3)_3.6H_2O$	99.99%	Alfa Aesar
Zirconium dichloride oxide octahydrate.	$ZrOCl_2.8\ H_2O$	98%	Alfa Aesar

Table 2.2: list of chemicals used in synthesis

$La_2Zr_2O_7$ used in the present study was prepared by co precipitating lanthanum (III) nitrate hexa hydrate ($La(NO_3)_3$ .6H2O; Alfa Aesar) and zirconyl dichloride octahydrate ($ZrOCl_2$. $8H_2O$; Alfa Aesar) in stoichiometric amounts of 0.1M solutions of $La(NO_3)_3$ and $ZrOCl_2$. The mixture was added drop wise, simultaneously with a solution of NH_3 to doubly distilled water, the pH of which had been adjusted to 11 with NH_3. A white gelatinous precipitate is formed during a vigorous stirring. The white precipitate was aged in the mother liquor for 24 h. The resultant gelatinous precipitate was then washed with a distilled water– NH_3 to obtain a material free of chloride and nitrate ions. The water-washed sample then was washed with ethanol and dried in an oven at 100°C for 24 h. The dried precipitate was dry-milled to obtain the powder sample. This powdered sample was annealed at 850°C for 4hrs

2.3.1.Temperature program

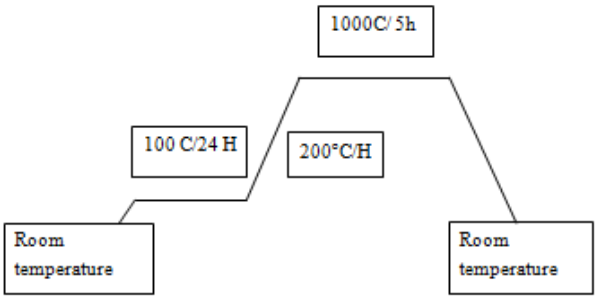

Fig 2.2.Temperature program for the synthesis of precursor.

2.4 Spray Pyrolysis – Coating Preparation

2.4.1 Spray Pyrolysis Apparatus

The spray pyrolysis apparatus used in this work has been designed and built at Periyar Maniammai University by PhD candidate Mr.Kesavan, and a schematic drawing of the apparatus is shown in Figure 2.3,2.4. The precursor solution was mixed with a synthetic carrier gas in the nozzle and sprayed onto a heated substrate as an aerosol. The substrate was heated up by a heating plate connected to a thermocouple controller. The spray unit could be moved accordingly to change the spraying distance and the pump controlled the volume and flow rate of the precursor solution. The heating plate was made of stainless Steel

At a given set-point temperature the substrate experienced different temperatures dependent on the spray pyrolysis conditions. The temperature on the heating plate, the temperature on the substrate with gas supply have been measured at different set-point temperatures. During spray pyrolysis both the gas and the liquid droplets cooled down the substrate. The temperature, the substrate was exposed to during spray pyrolysis was therefore slightly lower than the substrate temperature with gas supply. The temperature the substrate was exposed to during heat treatment or drying on the heating plate was the substrate temperature.

Fig 2.3. Spray pyrolysis apparatus (PMU- Dept of Physics)

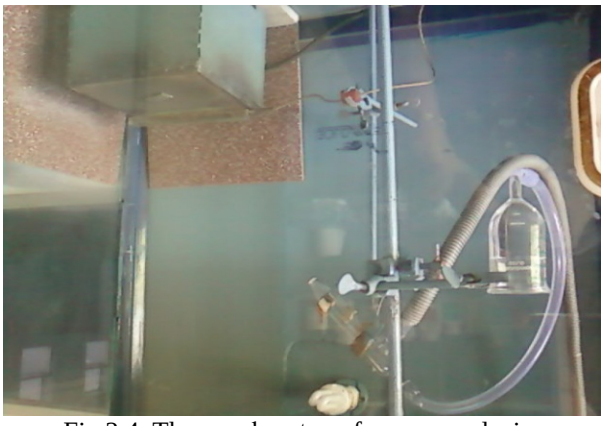

Fig 2.4. The nozzle setup of spray pyrolysis

2.4.2 Coating Composition and Precursor Concentration

Coatings of $La_2Zr_2O_7$ were deposited by spray pyrolysis. The unit used for concentration in this master thesis, shown in the column, is given in mol/L (M). The concentration of the precursor solution was adjusted by mixing the nitrate solution and the chloride solution according to stoichiometric before the solution was further diluted.

Coating	Concentration (mol/L)	Formula Weight	
		$La(NO_3)_3$ .6H2O	$ZrOCl_2$. $8H_2O$
$La_2Zr_2O_7$	0.1	433.01	322.25

Table 2.3: Molar concentration and FW of LZ

2.4.3 Spray Pyrolysis Parameters

Nozzle diameter – 0.3 micrometre

Pressure applied – 80-120 psi

Distance between the nozzle and the substrate- 31 cm

Spray time to standing time ratio- 5:15 Sec

III. RESULTS AND DISCUSSION

3.1 Thermal behavior

The results of the DTA and TGA analyses are shown in Fig. 15. The initial endothermic peak at ~90°C in the DTA trace is due to the loss of volatile water; two exothermic peaks at ~240°C and 450°C are probably due to the decomposition of ethanol.8 This corresponds to a continuous weight loss in the TGA trace up to a temperature of ~800°C. The final weight loss is ~24% of the initial sample weight. The exothermic peak at ~850°C in the DTA trace is due to the crystallization of $La_2Zr_2O_7$. The heat associated with this exothermic peak is 60 ± 3 kJ/mol^{-1}. To the best of our knowledge, there are no data available for $La_2Zr_2O_7$ on this aspect.

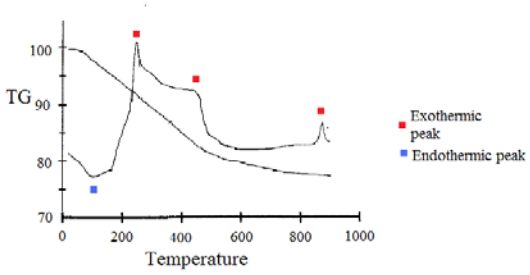

Fig 3.1. TGA/DTA curve of co precipitated LZ

3.2 Powder Characterization

To check the stoichiometric of the precursor solution, x-ray diffraction (XRD) measurements were performed on powder made from precursor solutions .

Precursor solutions with molar ratios of 1:1 of Lanthanum nitrate to Zirconium di chloride were heated to110 °C for 24 hours to evaporate the water. Each powder was crushed to small particles with a mortar . the powder was annealed at 1000 °C for four hours with heating and cooling rates of 200 °C/h. The Phase identification was performed with Ultima III Rigaku X-ray diffractometer at a scanning rate of 0.2°/min in the range of 5°- 60° with Cu K_α radiation (1.5406 Å). A solution of powder and ethanol was put on a Si single crystal sample holder and dried for 5 minutes to evaporate ethanol.

The diffractograms in Figure 16 present XRD results of $La_2Zr_2O_7$ powders made from precursor solutions with molar ratios of 1:1 is annealed at 1000 °C for 4 hours. The crystalline structure is started to form from amorphous after 600°C. before 600°C the sample formed is only amorphous. the peaks of the pyrochlore phase is detected in (222),(440),(622) and verified[17].on further heating the sample upto 1000°C, there is an increasing in intensity which denotes that there is an increase in crystallinity.

The particle sizes were calculated from the respective X-ray diffractograms using the Scherrer'sformula [6]:

$$t = k\lambda/B\cos\theta, \quad (1)$$

where t is the thickness in angstroms (Å) and corresponds to the diameter of particles assuming spherical shape, k is the wave length of the X-rays used, h is the Bragg's angle, and B is the full-width at half maximum measured in radians of the most intense line in the X-ray powder diffractogram. The size of the particles is found to be 215 Å for $La_2Zr_2O_7$. Reporters have reported the particle sizes as 102 Å by M.Vithal and 612 Å by Bhattacharya et al [7] which have been prepared at 900 °C.

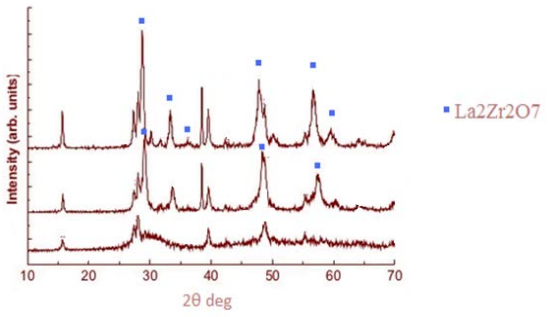

Fig 3.2.XRD pattern of LZ powder

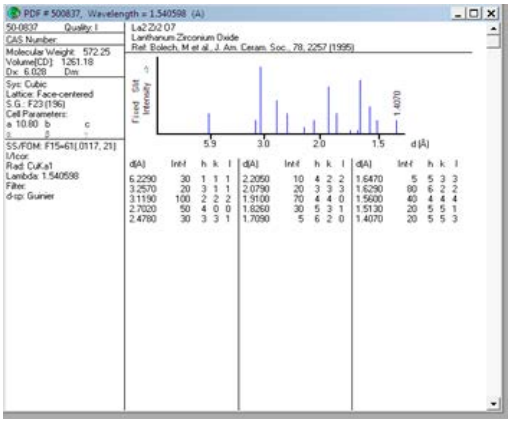

Fig 3.3.. JCPDS data file nos.: 17-450, 17-45

3.3 Surface Morphology

The microstructures of the surface of the coatings were analyzed using a scanning electron microscope (SEM) (VEGAS TESCAN) by secondary electron mode. The analysis of SEM micrographs is done for the bond coating, the amorphous LZ, the surface of the spray pyrolysed coating before and after thermal treatment.

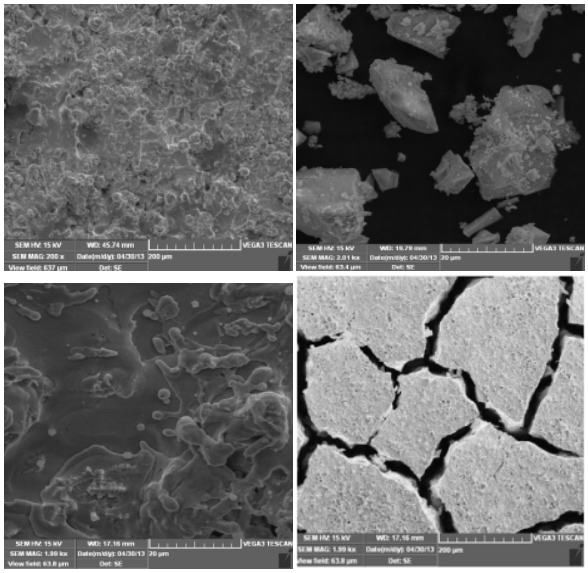

Fig 3.4. (a) NiCrAlY Bond coat over AISI310S, (b)$La_2Zr_2O_7$,(c) $La_2Zr_2O_7$ precursor coated over bond coating (before heat reatment),(d) $La_2Zr_2O_7$ precursor coated over bond coating(after heat treatment)

It is observed that the SEM image of the bond coating is non uniform. And from The particles of LZ is observed from fig. it is investigated that the particles observed are clustered. Structure of $La_2Zr_2O_7$ (*c-d*) coatings in the sprayed state before and, after 4h at 1000°C treatment. It is appeared that after the thermal treatment, there is the formation of cracks. The density and the size of the cracks might be higher due to the non uniform coating and also might be due to the possibilities of impurities present in LZ that has been observed in XRD analysis.

3.4.Thermo physical properties

3.4.1 Thermal expansion

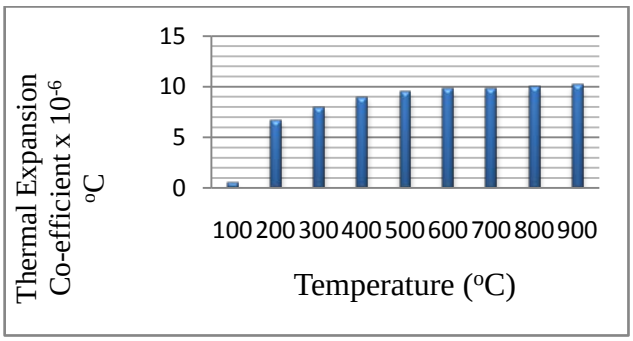

Fig 3.5. Graph of thermal expansion co effecient

The linear thermal expansion coefficients of $La_2Zr_2O_7$ are presented in Fig. 3.5, It can be seen that the linear thermal expansion coefficient of $La_2Zr_2O_7$ increase with the temperature increasing. The essence of the linear thermal expansion coefficient of solid materials increasing with the increase of temperature is that, the average distance between particles among the lattice increases with the temperature increasing. With the increasing of temperature, the crystal lattice vibration of solid materials is intensified, which results in the increase of the linear thermal expansion coefficient.

3.4.2. Specific heat

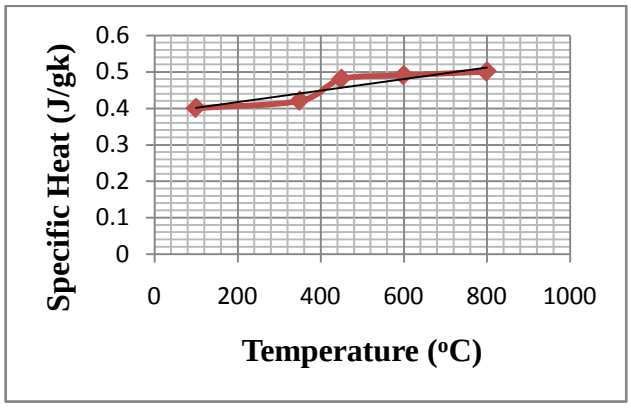

Fig 3.6. Graph of specific heat

The specific heats of $La_2Zr_2O_7$ for various temperatures are illustrated in Fig. 3.6, which indicates nearly a linear temperature dependence, i.e., $Cp \alpha T$, and increases with the temperature increasing. Due to the limitation of the measurement apparatus, the data of specific heat were determined only in the range between ambient and 800 ^oC.

3.4.3 Thermal diffusivity

The thermal diffusivities of $La_2Zr_2O_7$ decrease with the increasing of temperature in the range between ambient

and 800 ^{o}C, which is plotted in Fig. 21. shows an inverse temperature dependence, i.e., $\lambda \alpha T^{-1}$, in this temperature range. The T^{-1}-dependence diffusivity for $La_2Zr_2O_7$ suggests a dominant phonon conduction behavior, which resembles most polycrystalline materials [8].

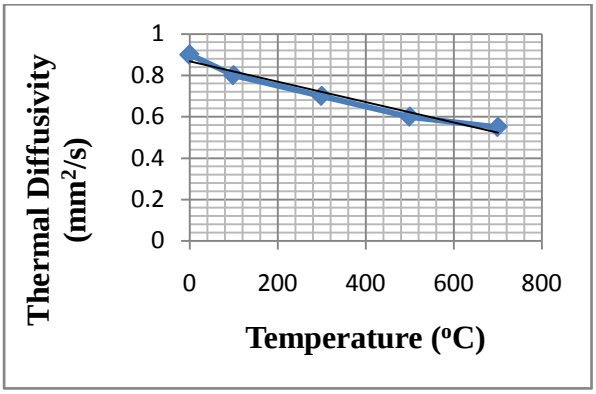

Fig 3.7.. Graph of thermal diffusivity

3.4.4. Thermal conductivity

The values of thermal conductivity are thus obtained by multiplying the thermal diffusivity, density and specific heat according to

$$k = Cp\ \lambda\ \rho \qquad (2)$$

It can be seen that thermal conductivity decreases gradually with the temperature increasing. According to the micro-mechanism of thermal conduction, the thermal conduction of inorganic non-metallic material is the results of phonon impacting. The thermal conductivity of phonon is shown as formula [9]

$$k = 1/3\ C_v\ v\ l \qquad (3)$$

where, *Cv* is the specific heat capacity of phonon, *v* is the average speed of phonon, *l* is the mean free path of phonon. *Cv* is almost a constant when temperature is upon Debye temperature. The value of *v* is related with elastic ratio (*E*) and density (*ρ*), because of the effect of temperature on the elastic ratio and density is not obviously, so the value of *v* may be also as a constant approximately.

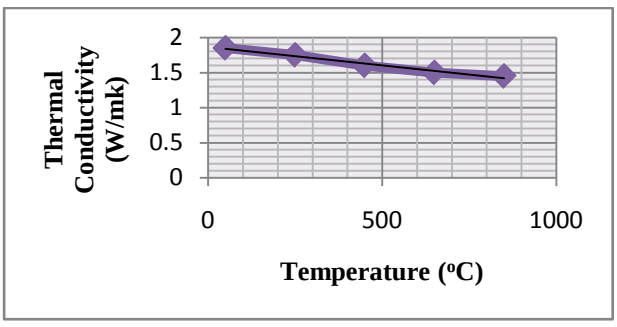

Fig 3.8. Graph of thermal condutivity

Consequently, the value of the crystal thermal conductivity (*k*) is decided by the law that the mean free path of phonon decreases with the increasing of temperature among most polycrystalline ceramic materials. With the increasing of temperature, the shaking energy of phonon increases, the frequency increases, the impact probability increases and the mean free path of phonon decreases, which results in the decrease of the thermal conductivity (*k*). This is the main reason of the thermal conductivity of most inorganic non-metallic materials decreases with the increasing temperature at upper temperature.

Low thermal conductivity is one of the most critical requirements for TBCs. The thermal conductivity of current 8YSZ is about 2.5 W/(m K) [10], which is higher than that LZ. It is well known that the substitution solid solution is formed by the substitution of Zr^{4+} cation by trivalent rare-earth cation when a trivalent rare-earth oxide is doped into ZrO_2 [11]. The substitution of two Zr^{4+} cations with two La^{3+} or Y^{3+} cations is accompanied by the incorporation of one oxygen vacancy, to maintain the electro neutrality of the lattice.

IV. CONCLUSION

LZ coatings have been deposited on stainless steel substrates by spray pyrolysis of an aqueous nitrate precursor solution. The influence of spray pyrolysed deposition of LZ and its thermo physical properties are investigated.

After the prepared ceramic powders were dry milled, Annealed, vacuum dried, molded by cold pressure and densified , the relative density of the LZ is 94.8 respectively. The linear thermal expansion coefficient of LZ is higher than that of 8YSZ when the temperature is over 400 ^{o}C, but the thermal conductivity of $La_2Zr_2O_7$ is much lower than that of 8YSZ. With the temperature increasing, the thermal expansion coefficient of the ceramics increased. Other thermo physical properties like specific heat , thermal diffusivity are also investigated. A linear temperature dependence of specific heat and inverse temperature dependence of thermal diffusivity is obtained.

It is concluded that with all these properties, with the increasing of temperature, the shaking energy of phonon increases, the frequency increases, the impact probability increases and the mean free path of phonon decreases, which results in the decrease of the thermal conductivity (*k*). This is the main reason of the thermal conductivity of most inorganic non-metallic materials decreases with the increasing temperature at upper temperature. The thermal conductivity obtained is 1.4 W/mk. Still researchers had stated that the thermal conductivity obtained from LZ by spray pyrolysis is lower than that of thermal spray i.e.

0.16-0.3 W/mk by spray pyrolysis and 0.8-1.7 W/mk by APS [12,13].

REFERENCES

[1]. N.P. Padture, M. Gell and E.H. Jordan, *Thermal Barrier Coatings for Gas-Turbine Engine Applications.* Science, 2002. 296: p. 280-284.

[2]. A. Feuerstein, J. Knapp, T. Taylor, A. Ashary, A. Bolcavage and N. Hitchman, *Technical and Economical Aspects of Current Thermal Barrier Coating Systems for Gas Turbine Engines by Thermal Spray and EBPVD: A Review*. Journal of Thermal Spray Technology, 2008. 17(2): p. 199-213.

[3]. D. W.Richerson, *Modern Ceramic Engineering Properties, Processing, and use in Design*. 3 ed. 2006: Taylor & Francis group.

[4]. X.Q. Cao, R. Vassen and D. Stoever, *Ceramic materials for thermal barrier coatings.* Journal of the European Ceramic Society, 2004. 24(1): p. 1-10

[5]. Skoog, Douglas A., F. James Holler and Timothy Nieman (1998). *Principles of Instrumental Analysis* (5 ed.). New York. pp. 805–808. ISBN 0-03-002078-6.

[6]. A.R. West, Solid State Chemistry and Its Applications, Wiley, New York, 1974, p. 172.

[7]. A.K. Bhattacharya, A. Hartridge, K.K. Mallick, J.L. Woodhead, Journal of Material Science 29 (1994) 6076.

[8]. W.D. Kingery, J. Am. Ceram. Soc. 38 (1955) 251.

[9]. M. R´emy, L. Jean-Claude, A. Alban, L. B´erang´ere, P. Martine, L. Odile,D. Didier, J. Eur. Ceram. Soc. 24 (2004) 3081.

[10]. D.M. Zhu, R.A. Miller, Ceram. Eng. Sci. Proc. 21 (2000) 623.

[11]. J. Wu, X.Z. Wei, N.P. Padture, P.G. Klemens, M. Gell, E. Garcia, J. Am.Ceram. Soc. 85 (2002) 3031.

[12]. N.P. Padture, M. Gell, E.H. Jordan, Science 296 (2002) 280.

[13]. Sophie B. Weber, Hilde L. Lein, Tor Grande, Mari-Ann Einarsrud," *Lanthanum zirconate thermal barrier coatings deposited by spray pyrolysis*" SCT-17989; No of Pages 5.